

Geometric Additivity of Modular Commutator for Multipartite Entanglement

Sung-Min Park,¹ Isaac H. Kim,^{2,*} and Eun-Gook Moon^{1,†}

¹*Department of Physics, Korea Advanced Institute of Science and Technology, Daejeon 34141, Korea*

²*Department of Computer Science, University of California, Davis, CA 95616, USA*

A recent surge of research in many-body quantum entanglement has uncovered intriguing properties of quantum many-body systems. A prime example is the modular commutator, which can extract a topological invariant from a single wave function. Here, we unveil novel geometric properties of many-body entanglement via a modular commutator of two-dimensional gapped quantum many-body systems. We obtain the geometric additivity of a modular commutator, indicating that modular commutator for a multipartite system may be an integer multiple of the one for tripartite systems. Using our additivity formula, we also derive a curious identity for the modular commutators involving disconnected intervals in a certain class of conformal field theories. We further illustrate this geometric additivity for both bulk and edge subsystems using numerical calculations of the Haldane and π -flux models.

Introduction: Two-dimensional gapped quantum systems exhibit intriguing many-body entanglement phenomena [1, 2]. A remarkable aspect of these systems is the bulk-edge correspondence, which dictates that the effective field theory at the boundary determines the universal properties of the bulk. A prime example is the quantum Hall effect in two spatial dimensions [3], where a nonzero bulk Chern number indicates the presence of gapless edge modes [4, 5]. These gapless edge modes can be characterized by the chiral central charge (c_-), which appears in the zero-temperature limit of the thermal Hall conductivity [5–7]. The bulk-edge correspondence suggests that the bulk ground state wave function may capture the chiral central charge, although how to extract it had remained puzzling.

Recently, Refs. [8–12] demonstrated that the modular commutator of the ground state can capture the chiral central charge. Let us recall the definition of a modular commutator

$$J(A, B, C) \equiv i \text{Tr}(\rho_{ABC}[K_{AB}, K_{BC}]),$$

where $K_X \equiv -\ln \rho_X$ is the modular Hamiltonian of the reduced density matrix ρ_X on region X . For the ground state of a two-dimensional gapped system, $|\Psi\rangle$, the modular commutator gives the chiral central charge [8–12]:

$$J(A, B, C) = \frac{\pi}{3} c_- \quad (1)$$

A tripartition ABC with a complete tri-junction is illustrated in Fig. 1(a). This result can be viewed as a part of an ongoing research program that aims to study universal properties of the underlying quantum many-body system via multipartite entanglement [13–19]. These recent developments call for further studies to explore the multipartite entanglement properties of many-body quantum systems.

In this paper, we extend the applicability of the modular commutator to more general geometries. Our work unveils a new universal geometric identity for the modular commutator. In particular, we find the curious identity that involves disconnected intervals in conformal field

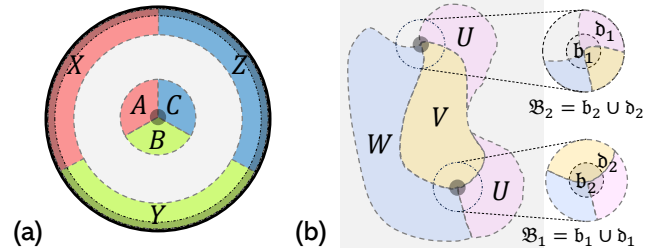


FIG. 1. Exemplary partitions in two-dimensional systems. (a) Tripartite bulk disk ABC and edge annulus XYZ . The shaded region represents the *physical* edge of the system. (b) Multipartite bulk partition with the subregions U, V, W . Two tri-junctions of (U, V, W) consist of two set of ‘balls’, $\mathfrak{B}_1 = \mathfrak{b}_1 \cup \mathfrak{d}_1$ and $\mathfrak{B}_2 = \mathfrak{b}_2 \cup \mathfrak{d}_2$.

theories (CFTs) and singular regions in the bulk. The geometric aspects of the modular commutator of multipartite entanglement are illustrated by employing the area law of entanglement entropy [20, 21] and numerical calculations of lattice models.

Geometric Additivity: Originally, the modular commutator [8, 9] was defined over a region partitioned into three disks, all meeting at a single tri-junction. We consider a more general partition that goes beyond this original setup. An example of such a system is shown in Fig. 1(b), which features two tri-junctions. We find that the modular commutator for such subsystems can be expressed as:

$$J(U, V, W) = \sum_i J(U_{\mathfrak{B}_i}, V_{\mathfrak{B}_i}, W_{\mathfrak{B}_i}) + J(U_{\mathfrak{r}}, V_{\mathfrak{r}}, W_{\mathfrak{r}}), \quad (2)$$

where an index i specifies a tri-junction of a subregion UVW . At each tri-junction, $V_{\mathfrak{B}_i} = V \cap \mathfrak{B}_i$ is for the intersection between a subregion V and a ball \mathfrak{B}_i . For an each ball \mathfrak{B}_i , a smaller ball \mathfrak{b}_i and an associated annulus region \mathfrak{d}_i are introduced to zoom in a tri-junction, $\mathfrak{B}_i = \mathfrak{b}_i \cup \mathfrak{d}_i$. A relative complement region of all the tri-junctions is defined as $V_{\mathfrak{r}} = V \setminus (\cup_i \mathfrak{b}_i)$, which contributes to the residual term, $J(U_{\mathfrak{r}}, V_{\mathfrak{r}}, W_{\mathfrak{r}})$. It then follows that

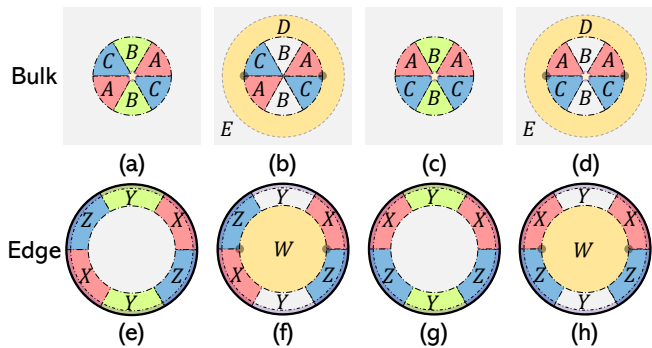


FIG. 2. Bulk and edge pizza partitions and corresponding multipartite subsystems. (a),(c) The bulk pizza partitions of ABC . (b),(d) The corresponding multipartite subsystems of (a) and (c), respectively. (e),(g) The edge pizza partitions of XYZ . (f),(h) The corresponding multipartite subsystems of (e) and (g), respectively.

$J(U_{\mathfrak{B}_i}, V_{\mathfrak{B}_i}, W_{\mathfrak{B}_i})$ is quantized as in Eqn. (1) for a complete junction, while an incomplete junction gives a non-quantized value. See Supplemental Materials (SM) for more details.

The modular commutator satisfies *geometric additivity* if the residual term vanishes. We prove that the residual term indeed vanishes for invertible states by using properties of quantum Markov chains and the area law of the entanglement entropy [20, 21]. For non-invertible states (e.g., states that can host anyons), it is an open question whether the geometric additivity holds in general. We provide a conjecture from which the additivity would follow, though the proof of it remains open; see SM for more details.

Applications: One of the main applications of geometric additivity is an exact calculation of the modular commutator for new types of subsystems. As an example, we consider a partition in Fig. 2(a), which we call as the pizza partition. Let us first consider a bulk system CDA in Fig. 2(b) with the complementary property $K_X|\Psi\rangle = K_{\bar{X}}|\Psi\rangle$. The modular commutator for CDA becomes

$$\begin{aligned} J(C, D, A) &= i\langle\Psi|[K_{ABE}, K_{BCE}]\Psi\rangle \\ &= i\langle\Psi|[K_{AB}, K_{BC}]\Psi\rangle = J(A, B, C), \end{aligned} \quad (3)$$

where in the second line, we use the fact that the state on the two sufficiently distant regions is a product state; for example, $K_{EAB} = K_E + K_{AB}$. Thus, we can use $J(C, D, A)$ to determine $J(A, B, C)$. Using the additivity formula we obtain

$$J(A, B, C) = 2 \times \frac{\pi}{3} c_- \quad (4)$$

for Fig. 1(a). In essence, each complete tri-junction of $J(C, D, A)$ contributes to the modular commutator (by $\frac{\pi}{3} c_-$), yielding a result that is twice as large as the one for

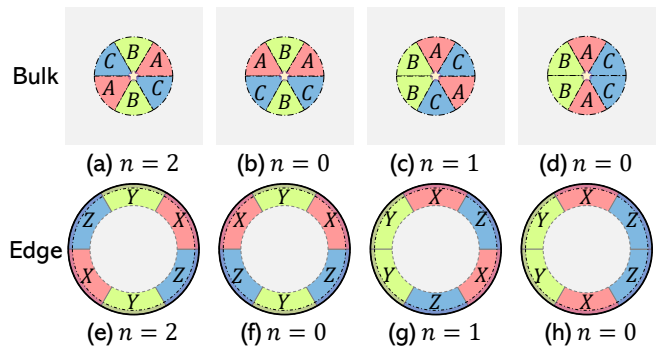


FIG. 3. The geometric integer n for the various bulk and edge pizza partitions.

the tripartition in Fig. 1(a). Similarly, one can apply the additivity formula to the pizza partition in Fig. 2(c), and show $J(A, B, C) = 0$. This is because the contributions from the two tri-junctions cancel each other out.

The additivity formula may also be applied to the physical edge of the system. The similar use of complementary property gives $J(X, Y, Z) = J(Z, W, X)$, and one can apply the additivity to the complement region. For example, for the pizza partition in Fig. 2(e), we find

$$J(X, Y, Z) = -2 \times \frac{\pi}{3} c_-. \quad (5)$$

We note that the modular Hamiltonians involved in the calculation of $J(X, Y, Z)$ are associated with disconnected intervals (e.g., XY and YZ). This is very different from the setup considered in Ref. [10], which only involved intervals. While the entanglement Hamiltonian for an interval is local [22], the entanglement Hamiltonian for disconnected intervals is not [23]. Our result shows that, in spite of this nonlocality, its modular commutator result in a substantially simpler form. However, our derivation only applies only to the edge theory of invertible states. It is currently unclear if Eqn. (5) holds for any 1+1D CFTs.

The geometric additivity can be further applied to various pizza partitions as in Fig. 3. It is straightforward to show that the modular commutators of a pizza partition yield

$$J(A, B, C) = -J(X, Y, Z) = \frac{\pi}{3} (c_- \times n), \quad n \in \mathbb{Z}, \quad (6)$$

where the arrangement of the bulk and edge pizza partition, ABC and XYZ , are topologically equivalent. The chiral central charge c_- is determined by a ground state $|\Psi\rangle$, and the integer n depends on the arrangement near the tri-junction. We refer to it as the *geometric integer* in this work. We conjecture that Eqn. (6) holds for most two-dimensional gapped systems, although our proof is limited to invertible states.

Lastly, we discuss the application of the additivity formula for incomplete junctions. An incomplete tri-

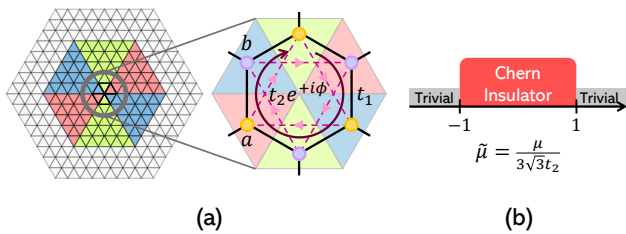


FIG. 4. Schematic description of the Haldane model (a) Upside-down triangles (∇) and triangles (\triangle) represent sublattices a and b , respectively. See the main text for the information on hopping parameters. (b) The phase diagram of the Haldane model. In the chern insulator phase at $-1 < \tilde{\mu} < 1$, chiral central charge is $c_- = 1$, otherwise zero.

junction generally exhibits non-quantized values dependent on microscopic details [11]. Yet, we find that the modular commutator with an incomplete junction has intriguing complementary properties. Namely, for a disk-like region $ABCD$, the sum of two modular commutators with incomplete junctions yields the following complementary relation:

$$\begin{array}{c} \text{B} \\ \text{C} \quad \text{A} \\ \text{D} \end{array} \quad J(A, B, C) + J(B, C, D) = \frac{\pi}{3} c_-, \quad (7)$$

where the subregion A, B, C, D meet at a point. This is an immediate consequence of geometric additivity. Interestingly, this identity holds even for non-invertible states, i.e., topologically ordered states that can host anyons; see the SM. Note that this complementary relation can be viewed as a bulk analog of the CFT identity recently discovered in Refs. [10, 11, 24]. A particular application of this identity arises when the system exhibits proper spatial symmetry near its tri-junction. This allows us to extract the chiral central charge within a smaller system size, yielding a *half*-quantized value: $J(A, B, C)_\sigma = J(B, C, D)_\sigma = \frac{1}{2} \times \frac{\pi}{3} c_-$.

Numerical calculation: We numerically verify the geometric additivity for certain lattice models. We consider the Haldane model on the honeycomb lattice [25], whose Hamiltonian consists of three parts:

$$H_H = H_0(\mu) + H_1(t_1) + H_2(t_2; \phi).$$

The first term contains the on-site energy terms with strength μ . We set the onsite energy to be μ for a sublattice and $-\mu$ for b sublattice: $H_0(\mu) = \mu \sum_r (c_{r,a}^\dagger c_{r,a} - c_{r,b}^\dagger c_{r,b})$. The second term H_1 includes the nearest-neighbor hopping terms with amplitude t_1 , which are represented as black solid links in Fig. 4(a): $H_1(t_1) = t_1 \sum_{\langle j,k \rangle} c_j^\dagger c_k$. The last term has the next nearest neighbor hopping terms with complex amplitude t_2 with phase ϕ , which breaks the time-reversal symmetry: $H_2(t_2; \phi) =$

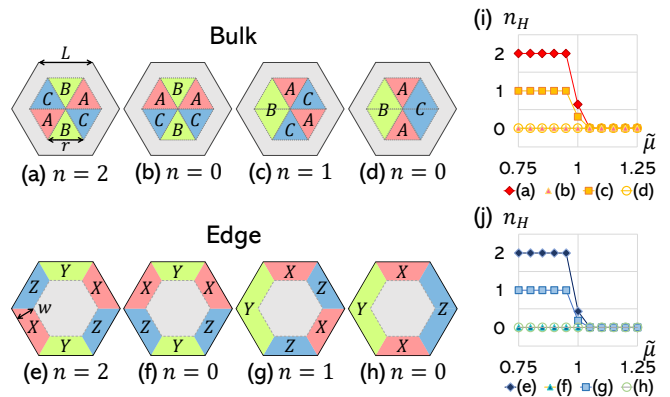


FIG. 5. Numerical evaluation of the geometric integer (n_H) for the pizza partitions. (a)-(h) The lattice realizations of the pizza partitions. We fix the linear system size L , bulk subsystem size r , and the edge width w : $L = 24$, $r = 17$, and $w = 13$. (i) Plot of n_H for the bulk pizza partitions with the tuning parameter $\tilde{\mu}$. (j) Plot of n_H for the edge pizza partitions with the tuning parameter $\tilde{\mu}$.

$|t_2| \sum_{\langle\langle j,k \rangle\rangle} e^{-i\phi\nu_{jk}} c_j^\dagger c_k$. Here, ν_{jk} are ± 1 and depends on the arrow's direction. The dashed arrows in Fig. 4(a) denote the next nearest hopping. The hopping in the direction of the arrow accumulates the flux ϕ . Setting a tuning parameter $\tilde{\mu} = \mu/(3\sqrt{3}t_2)$ with $t_1 = t_2 = 1$, we choose a one-dimensional path along $\phi = \pi/2$ where two topological phase transitions are present as in Fig. 4(b). It is well known that the Haldane model has the chiral central charge $c_- = 1$ for $-1 < \tilde{\mu} < 1$ and $c_- = 0$ for $\tilde{\mu} > 1$ and $\tilde{\mu} < -1$.

To evaluate its modular commutator, we divide the bulk lattice system into six sectors for a pizza partition. For example, a lattice realization of the bulk ABC is shown in Fig. 4(a). Note that the total number of lattice points in the pizza partition is 867, which makes each sector large enough except at the critical points at $\tilde{\mu} = \pm 1$.

The exact ground state of the Haldane model, $|\psi_H\rangle$, is readily obtained with a given lattice, and its modular commutator is numerically evaluated,

$$n_H \equiv \frac{3}{\pi} J(A, B, C) = i \frac{3}{\pi} \langle \psi_H | [K_{AB}, K_{BC}] | \psi_H \rangle. \quad (8)$$

The numerical values of n_H for the bulk pizza partitions, Fig. 5(a)-(d), are illustrated in Fig. 5(i) while the ones of $n_H = -\frac{3}{\pi} i \langle \psi_H | [K_{XY}, K_{YZ}] | \psi_H \rangle$ for the edge pizza partitions, Fig. 5(e)-(f), are illustrated in Fig. 5(j). We emphasize that the numerical calculations of n_H are precisely matched with the results of the geometric additivity away from the critical points ($\tilde{\mu} = \pm 1$).

To check the validity of our results, we also introduce small disorder to our numerical calculations by adding the Anderson term [26], $\sum_j V_j c_j^\dagger c_j$, where V_j is

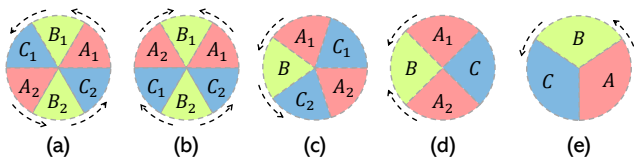


FIG. 6. The modular current interpretation for the pizza partitions. The non-trivial modular current of $J(A, B, C)$ flows from the subregions of AB into the subregions BC in the vicinity of their boundaries. (a)-(d) The pizza partitions of Fig. 2. (e) The pizza partition of the typical tri-junction as in Fig. 1(a).

sampled from a uniform distribution within the range $[-W/2, W/2]$. We choose W as 10% of the bulk energy gap, and no differences in the numerical calculations are found. We also perform similar calculations for the π -flux model on the square lattice and obtain qualitatively similar results for the higher geometric integers $n_\pi = 3, 4$. These results are presented in the SM.

Discussion and conclusion: Intuitively, the geometric integer n can be understood in terms of the modular current [5, 8, 9]. For any two regions L and R , this is defined as $f(L, R) = \sum_{v \in L} \sum_{u \in R} \tilde{f}_{vu}$, where $\tilde{f}_{vu} = i \langle [\tilde{K}_v, \tilde{K}_u] \rangle$ and \tilde{K}_v is the local modular Hamiltonian such that $K_X = \sum_{v \in X} \tilde{K}_v$. It is well understood that non-trivial modular current flows along the boundaries of nearby regions [8, 9].

We can apply this intuition to the bulk pizza partitions, reproducing the results we have shown rigorously. Due to the locality of the bulk modular Hamiltonian, the modular commutator may be rewritten as

$$J(A, B, C) = \sum_{v \in AB} \sum_{u \in BC} \tilde{f}_{vu}.$$

Thus, the modular current can be evaluated as a sum of current flowing from a subregion of AB to another subregion of BC . For instance, consider the partition of Fig. 6(a), where the subregion is written as $ABC = A_1 B_1 C_1 A_2 B_2 C_2$. The modular current has contributions from the four boundaries, (A_1, B_1) , (B_1, C_1) , (A_2, B_2) , (B_2, C_2) . Thus, the geometric integer is twice as large as the one of Fig. 6(e). We can apply a similar reasoning to the other pizza partitions, which yields results consistent with our analysis based on the geometric additivity.

To conclude, we posit a new geometric property of many-body quantum entanglement in two-dimensional gapped quantum many-body systems. This is the geometric additivity of the modular commutator, which indicates that modular commutator for subsystems more general than the one considered in Ref. [8, 9, 14] can be decomposed into a sum of modular commutators over simplified subsystems (e.g., involving balls or intervals). Numerical calculations of the Haldane model corroborate the geometric additivity, both in the bulk and at the edge.

We remark that a recent work [27] reported spurious contributions of modular commutators. In our numerical calculations, we have not observed such contributions, which is consistent with the previous work on the chiral central charge of free fermion models [12]. In future works, it would be desirable to develop a different method for extracting the chiral central charge which is free of such problems. One interesting question is whether the additivity can be proved rigorously for free fermion models.

Another important question is whether the geometric additivity holds for non-invertible states. We note that the additivity can be proved for a certain (non-vacuum) reduced density matrix that contains anyons; see the SM. However, how to relate this result to the state of interest, i.e., the vacuum-reduced density matrix, is unclear at the moment.

Acknowledgement: We thank K. Hwang, J. McGreevy, X. Li, T.-C. Lin, and B. Shi for helpful discussions. IK acknowledges support from NSF under award number PHY-2337931. S.-M.P. and E.-G.M. were supported by 2021R1A2C4001847, 2022M3H4A1A04074153, National Measurement Standard Services and Technical Services for SME funded by Korea Research Institute of Standards and Science (KRISS - 2024 - GP2024-0015) and the Nano & Material Technology Development Program through the National Research Foundation of Korea(NRF) funded by Ministry of Science and ICT(RS-2023-00281839).

* ikekim@ucdavis.edu

† egmoon@kaist.ac.kr

- [1] S. Sachdev, *Quantum Phases of Matter* (Cambridge University Press, 2023).
- [2] X.-G. Wen, *Quantum field theory of many-body systems: from the origin of sound to an origin of light and electrons* (OUP Oxford, 2004).
- [3] K. v. Klitzing, G. Dorda, and M. Pepper, New method for high-accuracy determination of the fine-structure constant based on quantized hall resistance, *Phys. Rev. Lett.* **45**, 494 (1980).
- [4] Y. Hatsugai, Chern number and edge states in the integer quantum hall effect, *Phys. Rev. Lett.* **71**, 3697 (1993).
- [5] A. Kitaev, Anyons in an exactly solved model and beyond, *Annals of Physics* **321**, 2 (2006), january Special Issue.
- [6] C. L. Kane and M. P. A. Fisher, Quantized thermal transport in the fractional quantum hall effect, *Phys. Rev. B* **55**, 15832 (1997).
- [7] N. Read and D. Green, Paired states of fermions in two dimensions with breaking of parity and time-reversal symmetries and the fractional quantum hall effect, *Phys. Rev. B* **61**, 10267 (2000).
- [8] I. H. Kim, B. Shi, K. Kato, and V. V. Albert, Chiral central charge from a single bulk wave function, *Phys. Rev. Lett.* **128**, 176402 (2022).

- [9] I. H. Kim, B. Shi, K. Kato, and V. V. Albert, Modular commutator in gapped quantum many-body systems, *Phys. Rev. B* **106**, 075147 (2022).
- [10] Y. Zou, B. Shi, J. Sorce, I. T. Lim, and I. H. Kim, Modular commutators in conformal field theory, *Phys. Rev. Lett.* **129**, 260402 (2022).
- [11] R. Fan, From entanglement generated dynamics to the gravitational anomaly and chiral central charge, *Phys. Rev. Lett.* **129**, 260403 (2022).
- [12] R. Fan, P. Zhang, and Y. Gu, Generalized real-space Chern number formula and entanglement hamiltonian, *SciPost Phys.* **15**, 249 (2023).
- [13] H. Dehghani, Z.-P. Cian, M. Hafezi, and M. Barkeshli, Extraction of the many-body chern number from a single wave function, *Phys. Rev. B* **103**, 075102 (2021).
- [14] Y. Zou, K. Siva, T. Soejima, R. S. K. Mong, and M. P. Zaletel, Universal tripartite entanglement in one-dimensional many-body systems, *Phys. Rev. Lett.* **126**, 120501 (2021).
- [15] K. Siva, Y. Zou, T. Soejima, R. S. K. Mong, and M. P. Zaletel, Universal tripartite entanglement signature of un-gappable edge states, *Phys. Rev. B* **106**, L041107 (2022).
- [16] R. Fan, R. Sahay, and A. Vishwanath, Extracting the quantum hall conductance from a single bulk wave function, *Phys. Rev. Lett.* **131**, 186301 (2023).
- [17] R. Kobayashi, T. Wang, T. Soejima, R. S. K. Mong, and S. Ryu, Extracting higher central charge from a single wave function, *Phys. Rev. Lett.* **132**, 016602 (2024).
- [18] R. Kobayashi, T. Wang, T. Soejima, R. S. K. Mong, and S. Ryu, Higher hall conductivity from a single wave function: Obstructions to symmetry-preserving gapped edge of (2+1) d topological order, *arXiv preprint arXiv:2404.10814* (2024).
- [19] S. Liu, Anyon quantum dimensions from an arbitrary ground state wave function, *Nature Communications* **15**, 5134 (2024).
- [20] A. Kitaev and J. Preskill, Topological entanglement entropy, *Phys. Rev. Lett.* **96**, 110404 (2006).
- [21] M. Levin and X.-G. Wen, Detecting topological order in a ground state wave function, *Phys. Rev. Lett.* **96**, 110405 (2006).
- [22] J. Cardy and E. Tonni, Entanglement hamiltonians in two-dimensional conformal field theory, *Journal of Statistical Mechanics: Theory and Experiment* **2016**, 123103 (2016).
- [23] R. E. Arias, H. Casini, M. Huerta, and D. Pontello, Entropy and modular hamiltonian for a free chiral scalar in two intervals, *Phys. Rev. D* **98**, 125008 (2018).
- [24] I. H. Kim, X. Li, T.-C. Lin, J. McGreevy, and B. Shi, Conformal geometry from entanglement, *arXiv preprint arXiv:2404.03725* (2024).
- [25] F. D. M. Haldane, Model for a quantum hall effect without landau levels: Condensed-matter realization of the "parity anomaly", *Physical review letters* **61**, 2015 (1988).
- [26] P. W. Anderson, Absence of diffusion in certain random lattices, *Phys. Rev.* **109**, 1492 (1958).
- [27] J. Gass and M. Levin, Many-body systems with spurious modular commutators, *arXiv preprint arXiv:2405.15892* (2024).
- [28] B. Shi, K. Kato, and I. H. Kim, Fusion rules from entanglement, *Annals of Physics* **418**, 168164 (2020).
- [29] Intuitively, it might be convenient to view this state as a ground state of a gapped Hamiltonian, though we do not make use of that fact.
- [30] D. Petz, Monotonicity of quantum relative entropy revisited, *Reviews in Mathematical Physics* **15**, 79 (2003).
- [31] I. Peschel and V. Eisler, Reduced density matrices and entanglement entropy in free lattice models, *Journal of physics a: mathematical and theoretical* **42**, 504003 (2009).
- [32] Note that the subsystem CDA is not a true two-hole disk, and its information convex set is not well-defined due to its bowtie shape (\bowtie). However, conditional independence remains true because of the strong subadditivity.

CONTENTS

References	4
A. Geometric additivity of a modular commutator	6
1. Setup: area law of the entanglement entropy	6
2. Derivation: geometric additivity formula	6
B. Geometric additivity of modular commutator for the incomplete disk	8
1. Summary of the results	8
2. Numerical Calculations and Remarks	8
C. Additional numerical calculations for π -flux model	9
1. Model Hamiltonian	9
2. Numerical results	10
D. Absence of the residual term in the invertible states and remarks on the non-invertible states	10
1. Proof: Absence of the residual term in the invertible bulk	10
2. Discussion: non-invertible bulk	11

The Supplementary Material is organized as follows. Section **A** provides the basic setup and a derivation of the geometric additivity formula. We provide another type of additivity formula for the incomplete disk in Section **B**. Section **C** presents results of numerical calculations on the π -flux model, including incomplete disk and $n \geq 3$ disconnected edge intervals. In Section **D**, we discuss the modular commutator of the pizza partition for invertible states and also provide remarks for the non-invertible states.

Appendix A: Geometric additivity of a modular commutator

In this Section, we derive the geometric additivity formula using the area law of entanglement entropy [20, 21], or equivalently, the entanglement bootstrap axiom **A1** [28].

1. Setup: area law of the entanglement entropy

The entanglement bootstrap [28] starts with two axioms on the entanglement entropy of the bulk ball \mathfrak{B} [Fig. 7(b)]:

$$\mathbf{A0}: \quad \Delta(B, C)_\sigma = 0, \quad (\text{A1a})$$

$$\mathbf{A1}: \quad \Delta(B, C, D)_\sigma = 0, \quad (\text{A1b})$$

where the subscripts σ of the parentheses is a state satisfying the axioms [29] and Δ s are linear combinations of

entanglement entropies:

$$\Delta(B, C)_\rho := (S_{BC} + S_C - S_B)_\rho \geq 0, \quad (\text{A2a})$$

$$\Delta(B, C, D)_\rho := (S_{BC} + S_{CD} - S_B - S_D)_\rho \geq 0. \quad (\text{A2b})$$

Here, the subscript represents the relevant subsystem. For instance, $(S_{BC} + \dots)_\rho$ is a shorthand notation for $S(\rho_{BC}) + \dots$, where $S(\rho_{BC}) = -\text{Tr}(\rho_{BC} \ln \rho_{BC})$ is the von Neumann entropy. Note that two entropic combinations are always non-negative by the Araki-Lieb inequality and strong subadditivity (SSA).

An immediate consequence of Eqns. (A1) is that for *any* subsystem $A \subset \Lambda \setminus \mathfrak{B}$, σ_{ABC} forms a quantum Markov chain (with respect to the choice of B and C appearing in Eqns. (A2)). In other words, the conditional mutual information of a tripartite state σ_{ABC} — defined as $I(A : C|B)_\rho := (S_{AB} + S_{BC} - S_B - S_{ABC})_\rho$ — vanishes:

$$I(A : C|B)_\sigma = 0. \quad (\text{A3})$$

Moreover, the modular Hamiltonian ($K_X \equiv -\ln \rho_X$) for a quantum Markov states σ_{ABC} can be decomposed into the following form [30]:

$$I(A : C|B) = 0 \iff K_{ABC} = K_{AB} + K_{BC} - K_B. \quad (\text{A4})$$

By repeatedly applying the same argument, one can often decompose the modular Hamiltonian as a linear combination of terms that act on increasingly smaller subsystems [9].

2. Derivation: geometric additivity formula

In this subsection, we prove the geometric additivity of the modular commutator,

$$J(U, V, W) = \sum_i J(U_{\mathfrak{B}_i}, V_{\mathfrak{B}_i}, W_{\mathfrak{B}_i}) + J(U_\tau, V_\tau, W_\tau), \quad (\text{A5})$$

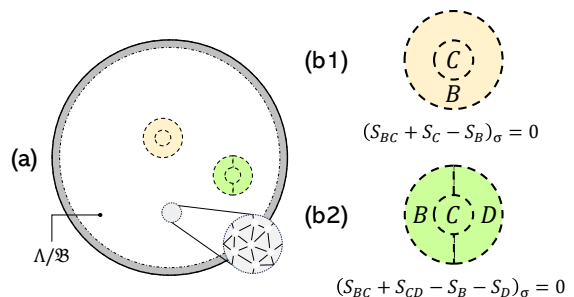


FIG. 7. Schematic descriptions on the two entropic axioms. (a) A gapped quantum many-body system Λ , and the bulk ‘ball’ regions \mathfrak{B} lying in the bulk. The solid lines at the edge represent the physical boundary, and the dashed lines represent the entanglement cut. (b) Two entropic combinations under area law. Subregions B , C , and D are sufficiently larger than the bulk correlation length.

\mathfrak{b}_j	a ball centered at j -th tri-junction
\mathfrak{d}_j	an annulus surrounding \mathfrak{b}_j , $\mathfrak{d}_j = \mathfrak{d}_{1,j} \cup \mathfrak{d}_{2,j}$
\mathfrak{B}_j	Union of \mathfrak{b}_j and \mathfrak{d}_j , $\mathfrak{B}_j = \mathfrak{b}_j \cup \mathfrak{d}_j$
\mathfrak{r}_j	The relative complement of \mathfrak{b}_j , <i>e.g.</i> $\mathfrak{r}_j = \Lambda/\mathfrak{b}_j$
\mathfrak{R}_j	The relative complement of \mathfrak{B}_j , <i>e.g.</i> $\mathfrak{R}_j = \Lambda/\mathfrak{B}_j$

TABLE I. Summary of notations (See also Fig. 8(b))

using entanglement bootstrap axiom **A1** [Eqn. (A1b)]. Throughout this subsection, we will use the notation summarized in Table. I and suppress the notation for σ unless it is unclear.

For concreteness, we consider an exemplary multipartite region U , V , and W [Fig. 8(a)]. This will be our guiding example for proving the additivity formula. We note that these specific regions are chosen only for pedagogical purposes. The proof itself can be generalized straightforwardly to other choices of subsystems. This is because our approach is to sequentially excise a ball that includes a tri-junction one by one; for any choice of subsystems, one can simply repeat the same procedure, arriving at the additivity formula [Eqn. (A5)].

The following are the key observations. First, we can apply axiom **A1** to a ball containing the tri-junction and thus decompose the modular Hamiltonian of UV and VW near the tri-junction [Eqn. (A4)]. For instance, consider the i -th tri-junction of the subregion VW and apply the axiom **A1**. Without loss of generality, we can decompose the modular Hamiltonian of VW near the tri-junction, thanks to Eqn. (A6):

$$I((VW)_{\mathfrak{b}_i} : (VW)_{\mathfrak{d}_{2,i}\mathfrak{R}_i} | (VW)_{\mathfrak{d}_{1,i}}) = 0, \quad (\text{A6})$$

where $\mathfrak{d}_{1,i}$ is the inner annulus surrounding \mathfrak{b}_i , and $\mathfrak{d}_{2,i}$ is the outer annulus surrounding $\mathfrak{d}_{1,i}$ [Fig. 8(b)]. The subscripts of VW denote the intersections. The second observation is that applying this decomposition yields contributions from additional tri-junctions, which exactly cancel each other out; see the two green-shaded regions in Fig. 8(b).

We now elaborate on these observations in more detail, focusing on a tri-junction of UVW . In what follows, we will obtain a succinct expression [Eqn. (A10)] for $J(U, V, W)$. We start by rewriting the modular commutator as

$$J(U, V, W) = i\langle [K_{UV}, K_{(VW)_{\mathfrak{b}\mathfrak{d}_1}}] \rangle - i\langle [K_{UV}, K_{(VW)_{\mathfrak{d}_1}}] \rangle + i\langle [K_{UV}, K_{(VW)_{\mathfrak{r}}}] \rangle. \quad (\text{A7})$$

All three terms are generally nonzero since they all have tri-junctions [green shaded regions in Fig. 8(b)]. However, we can judiciously cancel out some of those contributions using the quantum Markov chain, such as Eqn. (A6).

Let us compute the first line of Eqn. (A7).

$$\begin{aligned} & \langle [K_{UV}, K_{(VW)_{\mathfrak{b}\mathfrak{d}_1}}] \rangle - \langle [K_{UV}, K_{(VW)_{\mathfrak{d}_1}}] \rangle \\ &= \langle [K_{(UV)_{\mathfrak{B}}}, K_{(VW)_{\mathfrak{b}\mathfrak{d}_1}} - K_{(VW)_{\mathfrak{d}_1}}] \rangle \\ &= \langle [K_{(UV)_{\mathfrak{B}}}, K_{(VW)_{\mathfrak{B}}} \rangle - \langle [K_{(UV)_{\mathfrak{B}}}, K_{(VW)_{\mathfrak{d}}} \rangle, \end{aligned} \quad (\text{A8})$$

where in the second line of Eqn. (A8) we reduce the region UV into its restriction onto the ball \mathfrak{B} , by using an identity $\langle [K_{UV}, K_{(VW)_{\mathfrak{b}\mathfrak{d}_1}}] \rangle = \langle [K_{(UV)_{\mathfrak{B}}}, K_{(VW)_{\mathfrak{b}\mathfrak{d}_1}}] \rangle$. Using a similar identity, we extend the region \mathfrak{d}_1 of VW to $\mathfrak{d} = \mathfrak{d}_1 \cup \mathfrak{d}_2$ in the third line.

The second line of Eqn. (A7) can be also calculated similarly:

$$\begin{aligned} \langle [K_{UV}, K_{(VW)_{\mathfrak{r}}} \rangle &= \langle [K_{(UV)_{\mathfrak{b}\mathfrak{d}_1}} - K_{(UV)_{\mathfrak{d}_1}}, K_{(VW)_{\mathfrak{r}}} \rangle \\ &\quad + \langle [K_{(UV)_{\mathfrak{r}}}, K_{(VW)_{\mathfrak{r}}} \rangle \\ &= \langle [K_{(UV)_{\mathfrak{B}}} - K_{(UV)_{\mathfrak{d}}}, K_{(VW)_{\mathfrak{d}}} \rangle \\ &\quad + \langle [K_{(UV)_{\mathfrak{r}}}, K_{(VW)_{\mathfrak{r}}} \rangle, \end{aligned} \quad (\text{A9})$$

where in the first line, we used a decomposition of K_{UV} . For the first term of the second equality, we first reduce the region $(VW)_{\mathfrak{r}}$ to $(VW)_{\mathfrak{d}}$ and then extend the $(UV)_{\mathfrak{b}\mathfrak{d}_1}$ to $(UV)_{\mathfrak{B}}$.

Now that we have computed both lines of Eqn. (A7), let us collect those terms together. By combining Eqn. (A8) and Eqn. (A9), we obtain the following decomposition for the i 'th tri-junction:

$$J(U, V, W) = J(U_{\mathfrak{B}_i}, W_{\mathfrak{B}_i}, W_{\mathfrak{B}_i}) + J(U_{\mathfrak{r}_i}, V_{\mathfrak{r}_i}, W_{\mathfrak{r}_i}) - J(U_{\mathfrak{d}_i}, V_{\mathfrak{d}_i}, W_{\mathfrak{d}_i}). \quad (\text{A10})$$

The only difference between Eqn. (A10) and the additivity formula is [Eqn. (A5)] is the presence of an additional term $J(U_{\mathfrak{d}_i}, V_{\mathfrak{d}_i}, W_{\mathfrak{d}_i})$.

We note that this additional term is zero:

$$J(U_{\mathfrak{d}_i}, V_{\mathfrak{d}_i}, W_{\mathfrak{d}_i}) = 0. \quad (\text{A11})$$

This is because the two modular Hamiltonians over $(UV)_{\mathfrak{d}_i}$ and $(VW)_{\mathfrak{d}_i}$ can be written as a linear combination of local terms, whose resulting modular commutators are zero. (The modular commutators are zero due

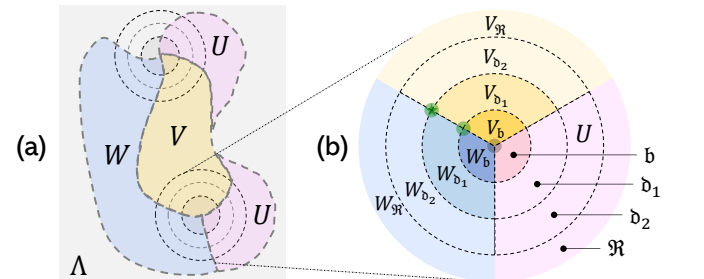


FIG. 8. (a) Exemplary multi-partition UVW in UVW in two-dimensional quantum many-body system Λ . (b) Schematic description of the i 'th ball region, $\mathfrak{B}_i = \mathfrak{b}_i \cup \mathfrak{d}_i$. The black and green shaded region are tri-junctions in Eqn. (A7).

to the quantum Markov chain structure.) Thus, we conclude Eqn. (A11). In particular, we obtain

$$J(U, V, W) = J(U_{\mathfrak{B}_i}, W_{\mathfrak{B}_i}, W_{\mathfrak{B}_i}) + J(U_{\tau_i}, V_{\tau_i}, W_{\tau_i}). \quad (\text{A12})$$

This procedure can be repeatedly applied for every tri-junction of $J(U, V, W)$, yielding the additivity formula:

$$J(U, V, W) = J(U_{\tau}, V_{\tau}, W_{\tau}) + \sum_i J(U_{\mathfrak{B}_i}, V_{\mathfrak{B}_i}, W_{\mathfrak{B}_i}),$$

where $\tau = \cup_i \tau_i$.

Below, we provide some remarks. First, Eqn. (A5) of the modular commutator holds even for incomplete tri-junctions because the observation used in the proof remains valid for incomplete junctions. Second, $J(U, V, W)$ is invariant under smooth bulk deformations away from the tri-junction. Here, smooth bulk deformation means deformations of subsystems within the modular commutator that do not add or remove the tri-junction. Finally, the modular commutator for the bulk residual term vanishes

$$J(U_{\tau}, V_{\tau}, W_{\tau}) = 0,$$

when the subsystems $(UV)_{\tau}$ and $(VW)_{\tau}$ are disk-shaped regions. This follows from the observation in Ref. [9] that the modular Hamiltonian for a disk-shaped bulk region can be expressed as a sum of local modular Hamiltonians. Therefore, for the disk-like regions, the modular commutator $J(U_{\tau}, V_{\tau}, W_{\tau})$ can be expressed as a sum of local modular commutators. Each of these commutators is a quantum Markov chain and always vanishes.

Appendix B: Geometric additivity of modular commutator for the incomplete disk

In this Section, we discuss another intriguing application of the additivity formula [Eqn. (A5)], the *incomplete disk* [11]. Let us consider a disk $ABCD$ shown in Fig. 9(a). Unlike previous cases, subregion A, B, C does not fully surround its tri-junction. We also call such tri-partitions ABC as the incomplete disk.

1. Summary of the results

For incomplete disks ABC and BCD , we find another type of additivity for modular commutators:

$$J(A, B, C) + J(B, C, D) = \frac{\pi}{3} c_{-}. \quad (\text{B1})$$

As an immediate consequence, four modular commutators of incomplete disk $ABCD$ have the following relations: $J(A, B, C) = J(C, D, A)$ and $J(B, C, D) = J(D, A, B)$.

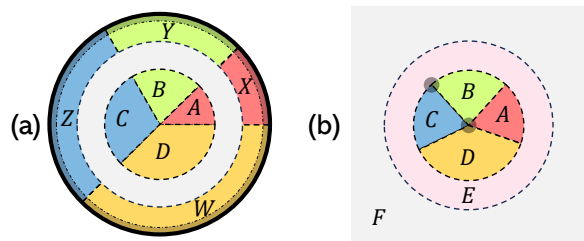


FIG. 9. Schematic descriptions for incomplete tri-junction. (a) Bulk disk $ABCD$ and edge annulus $XYZW$. (b) Partitions (A, B, C, D, E, F) for the proof of Eqn. (B1).

To prove it, let us consider partitions $BCDE$ illustrated in Fig. 9(b). We first switch the modular Hamiltonian of the subsystem CDE to ABF using the complementary property, $K_{CDE}|\Psi\rangle = K_{ABF}|\Psi\rangle$,

$$J(DE, C, B) = J(AF, B, C) = J(A, B, C). \quad (\text{B2})$$

where in the second equality, we use $K_{ABF} = K_{AB} + K_F$. Then, we apply the additivity formula to $J(DE, C, B)$, resulting in

$$J(DE, C, B) = J(E_{\mathfrak{B}}, C_{\mathfrak{B}}, B_{\mathfrak{B}}) + J(D_{\mathfrak{B}}, C_{\mathfrak{B}}, B_{\mathfrak{B}}) + J((DE)_{\tau}, C_{\tau}, B_{\tau}), \quad (\text{B3})$$

where two terms in the first line are nonvanishing terms, which are evaluated as follows

$$J(E_{\mathfrak{B}}, C_{\mathfrak{B}}, B_{\mathfrak{B}}) = \frac{\pi}{3} c_{-}, \quad (\text{B4a})$$

$$J(D_{\mathfrak{B}}, C_{\mathfrak{B}}, B_{\mathfrak{B}}) = J(D, C, B). \quad (\text{B4b})$$

The residual term in Eqn. (B3) has no triple point, and the modular Hamiltonian $K_{(BC)_{\tau}}$ is local, but $K_{(CDE)_{\tau}}$ is non-local. However, it can be easily verified

$$J((DE)_{\tau}, C_{\tau}, B_{\tau}) = 0, \quad (\text{B5})$$

once we appropriately decompose $K_{(BC)_{\tau}}$ into smaller three chunks by Eqn. (A4).

In conclusion, we obtain the geometric additivity of a modular commutator for the incomplete disk,

$$J(A, B, C) + J(B, C, D) = \frac{\pi}{3} c_{-}. \quad (\text{B6})$$

It states that the sum of two incomplete modular commutators is $\frac{\pi}{3} c_{-}$ if the union of tripartitions forms a complete disk.

2. Numerical Calculations and Remarks

We now test the formula (B1) for the Haldane model discussed in the main text. We choose two cases of disks $ABCD$, which are illustrated in Fig. 10(a-b) and (c-d).

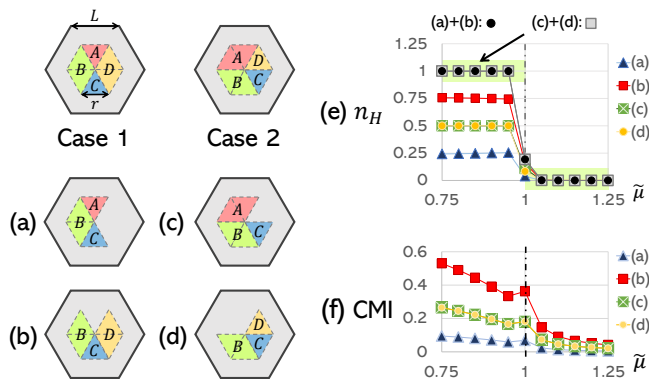


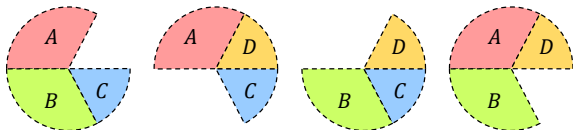
FIG. 10. Numerical evaluation of modular commutator for the incomplete disks. (a)-(d) The lattice realization of the incomplete disks. We fix the linear size of the system L , and the subsystem size r : $L = 22$ and $r = 15$. (e) Plot of $n_H \equiv \frac{3}{\pi}J$ of the Haldane model and the sum for the incomplete disks with tuning parameter $\tilde{\mu}$. (f) Plot of conditional mutual information (CMI) $I(A : C|B)$ for the incomplete disk with tuning parameter $\tilde{\mu}$.

For each case, the modular commutators are computed in the parameter range of $0.5 < \tilde{\mu} < 1.25$, as shown in Fig. 10(e). In both cases, the sum of two modular commutators of the incomplete disks yields $\frac{\pi}{3}c_-$, which is consistent with our arguments.

Below, we provide some remarks. The first remark is about the second case in Fig. 10. In the Chern insulator phase, (a) and (b) have different values. However, (c) and (d) are nearly identical despite the fact that two incomplete disks (ABC and BCD) are different. It indicates that we can extract an exact chiral central charge from an incomplete disk alone, yielding $\pi c_-/6$. This is due to the symmetry of the Haldane model, which enforces the following relation:

$$J(A, B, C) = J(B, C, D) = J(C, D, A) = J(D, A, B).$$

Specifically, if the partition of incomplete disks $ABCD$ is given as below,



and the system has a proper spatial symmetry, the two modular commutators $J(A, B, C)$ and $J(D, A, B)$ may be equal, resulting in $J(A, B, C) = J(B, C, D) = \frac{1}{2} \times \frac{\pi}{3}c_-$. This observation may be useful for extracting the chiral central charge more efficiently in numerical studies.

The second remark is about the incomplete tri-junction and the conditional mutual information. It is well-known that if a tripartite state ρ_{ABC} is a quantum Markov

chain, then the modular commutator vanishes,

$$I(A : C|B)_\rho = 0 \implies J(A, B, C)_\rho = 0. \quad (\text{B7})$$

Meanwhile, the tri-junction of an incomplete disk ABC , which makes a non-smooth boundary, provides a non-vanishing value of the conditional mutual information. Without the tri-junction, the conditional mutual information (CMI) of the incomplete disk becomes zero because of the area law, and the modular commutator is zero. We present the conditional mutual information of incomplete disks in Fig. 10(f), which are nonzero in the chiral topological phase and decrease in the trivial phase.

Lastly, one can view Eqn. (B1) as a bulk analog of an identity that is satisfied by the edge modular commutator [10, 11, 24]. For instance, the modular commutators at the contiguous edge intervals XYZ in Fig. 9(a) also satisfy the similar relation under exchanging XYZ to YZW : $J(X, Y, Z) = \frac{\pi}{3}c_- - J(Y, Z, W)$. A similar observation was made in Ref. [24].

Appendix C: Additional numerical calculations for π -flux model

This Section provides additional numerical calculations involving the π -flux model, which is a free fermion model. Since the ground state of the free fermion systems is the Gaussian state, the reduced density matrix and modular commutators are completely determined by their two-point correlation functions [31].

1. Model Hamiltonian

The π -flux models are defined on the square lattice, consisting of two sublattices, a and b . We use $j = (r, s)$ to label the unit cell r and the two sublattices $s = a, b$. The π -flux model is described by the following Hamiltonian:

$$H_\pi = H_1(t_1) + H_2(t_2; \phi) \quad (\text{C1})$$

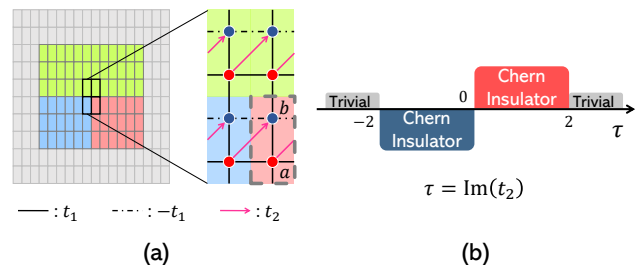


FIG. 11. Schematic description of π -flux model. (a) Each rectangle denotes the unit cell. See the main text for the details of hopping parameters. (b) Phase diagram of the π -flux model along $\tau = \text{Im}(t_2)$ -line. In topological phases, the chiral central charge is $c_- = 1$ at $0 < \tau < 2$, and $c_- = -1$ at $-2 < \tau < 0$.

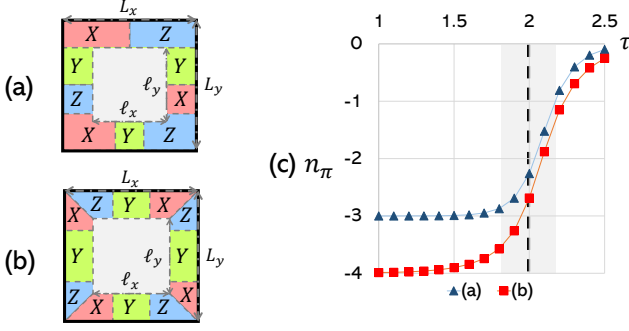


FIG. 12. Numerical evaluation of the geometric integer ($n \geq 3$) for the edge pizza partition. (a)-(b) The lattice realization of the edge pizza portions with $n = 3, 4$, respectively. We fix the system size $L_x = 47$, $L_y = 46$, and the $\ell_x = 27$, $\ell_y = 26$. (c) Plot of n_π for the edge pizza partition with the tuning parameter τ .

The first part concerns the nearest hopping Hamiltonian with amplitude t_1 , $H_1(t_1) = t_1 \sum_{\langle j,k \rangle} \eta_{jk} c_j^\dagger c_k$, which is illustrated as black links. We use black dashed links for hopping between two b sublattices, $\eta_{jk} = -1$, and black solid links for all the rest of hopping, $\eta_{jk} = 1$. The second part includes the next nearest hopping terms with complex amplitude t_2 , $H(t_2; \phi) = \tau \sum_r (i c_{r+\hat{x},b}^\dagger c_{r,a} + \text{h.c.})$, which are depicted as arrows in Fig. 11(a). Here, we choose the amplitude to be purely imaginary $t_2 = i\tau$.

In the π -flux model, we keep t_1 fixed at 1 and vary τ . The model exhibits two chiral topological and trivial phases along the τ -parametric path. The topological phase at $0 < \tau < 2$ has a chiral central charge of $c_- = 1$, while the other topological phase at $-2 < \tau < 0$ has opposite chiralities with a chiral central charge of $c_- = -1$. Outside of these ranges, the π -flux model is trivial.

2. Numerical results

We first consider the pizza partitions in the π -flux model with the geometric integer ($n \geq 3$). Since the model is defined on a lattice, verifying higher values of n in the bulk subsystem is not straightforward. For this reason, we only provide the numerical evaluations of the geometric integer for the edge pizza partitions, $n_\pi \equiv -\frac{3}{\pi} J(X, Y, Z)$ ($n \geq 3$). We select XYZ as shown in Fig. 12(a)-(b). Particularly for $n = 3$, we choose the lengths of each interval, X, Y , and Z , not equal. Numerical estimations of the geometric integers n_π are presented in Fig. 12(c). The geometric integers well-converge for a large energy bulk gap ($1 < \tau < 1.5$). As τ approaches the critical point, the values of the modular commutator start to break down due to the decreasing energy gap. This is because to be well-converged to the integer, each interval demands a larger size than the bulk correlation length.

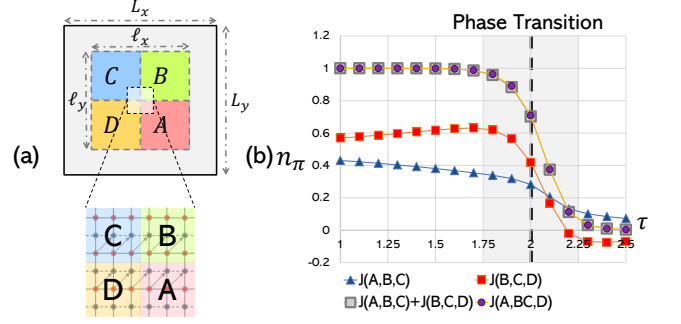


FIG. 13. Numerical evaluation of the modular commutator for the incomplete disk $ABCD$. (a) Incomplete disk $ABCD$ in π -flux model. We fix the disk size $(\ell_x, \ell_y) = (15, 14)$ and the system size $(L_x, L_y) = (47, 46)$. (c) Plot of modular commutators and the sum for the incomplete disks with the tuning parameter τ .

Next, we consider the π -flux model shown in Fig. 13. We choose a partition $ABCD$ of the π -flux model as depicted in Fig. 13(a). We compute the modular commutators at $1 < \tau < 2.5$ as shown in Fig. 13(b). Two modular commutators of the incomplete disks exhibit variations as the parameter τ changes. However, the sum always equals $J(A, BC, D)$, in both chiral topological and trivial phases. This is consistent with our discussion.

Appendix D: Absence of the residual term in the invertible states and remarks on the non-invertible states

In this Section, we prove the residual term of the additivity formula is absent for the invertible bulk. We also discuss the additivity for the non-invertible system.

1. Proof: Absence of the residual term in the invertible bulk

The main issue in evaluating the modular commutator of the pizza partition is that it has a non-trivial topology. For example, the subsystem of the bulk pizza partition has a bowtie shape (\bowtie); it is non-trivial whether it is a connected one region or disconnected two regions. These issues become subtle when the system is topologically ordered. However, based on the observations below, this issue can be circumvented for the invertible bulk.

For concreteness, let us consider a two-dimensional gapped system $ABCDE$ on a disk as shown in Fig. 14(a). The entanglement entropies of these subsystems are related as

$$I(A : C|B) + I(E : C|D) = \Delta(B, C, D), \quad (\text{D1})$$

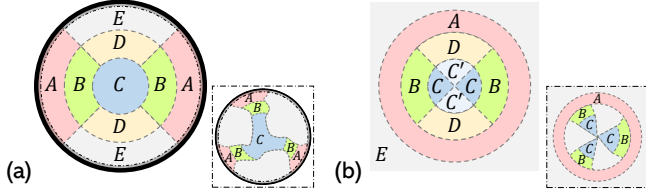


FIG. 14. Multipartite regions in a two-dimensional system. If the bulk is invertible, the conditional mutual information $I(A : C|B)$ vanishes for any smooth bulk deformation of ABC . (a) A, E are disconnected edge region at physical boundary, and BCD is bulk region. (b) A multipartite region $ABCC'D$ in the bulk.

where $\Delta(B, C, D) = S_{BC} + S_{CD} - S_B - S_D$ and we use $S_{AB} = S_{CDE}$ and $S_{ABC} = S_{DE}$ for pure state. The bulk subsystem BCD is similar to the partition for the axiom **A1** [Eqn. (A1b)], but the subsystem B and D are the union of the disconnected two regions. In this case, $\Delta(B, C, D)$ is no longer zero; rather, it gives the topological entanglement entropy (γ_{top}) [20, 21]: $\Delta(B, C, D) = 2\gamma_{\text{top}}$. Note that the topological entanglement entropy contribution in Δ depends on the number of the disconnected components of B (or D). For instance, if the B and D are the union of m disconnected region, then $\Delta(B, C, D) = 2(m-1)\gamma_{\text{top}}$.

A key observation of Eqn. (D1) is that if the bulk is invertible ($\gamma_{\text{top}} = 0$), the quantum state on the subsystem ABC is the quantum Markov state. Thus the modular Hamiltonian of ABC is local [30]:

$$K_{ABC} = K_{AB} + K_{BC} - K_B. \quad (\text{D2})$$

This observation can be further generalized. For example, if the bulk is invertible, we have $I(A : C|B) = 0$ for the partition ABC shown in the inset of Fig. 14(a), where the edge region A and the bulk region B consist of three disconnected regions.

One can also obtain similar results for the bulk multipartition $ABCC'D$ in Fig. 14(b). We find

$$I(A : C|B) + I(A : C'|D) = \Delta(B, CC', D). \quad (\text{D3})$$

Here, $\Delta(B, CC', D) = 2\gamma_{\text{top}}$ and we use the fact that the state in sufficiently distant regions is a product state, for example, $S_{AD} = S_{BCC'} + S_E$. It is clear that when the bulk is invertible ($\gamma_{\text{top}} = 0$), the modular Hamiltonian becomes local.

Below, we prove the absence of the residual term. While we focus on the examples in Fig. 15, the proof for the other cases is straightforward as well.

Let us first consider the edge residual term $J(Z_\tau, W_\tau, X_\tau)$ and let $W_\tau = W_1 W_2 W'$ as shown in Fig. 15(a). From Eqn. (D2), we have

$$\begin{aligned} K_{(ZW)_\tau} &= K_{Z_\tau W_2} + K_{W_\tau} - K_{W_2} \\ K_{(XW)_\tau} &= K_{X_\tau W_1} + K_{W_\tau} - K_{W_1} \end{aligned}$$

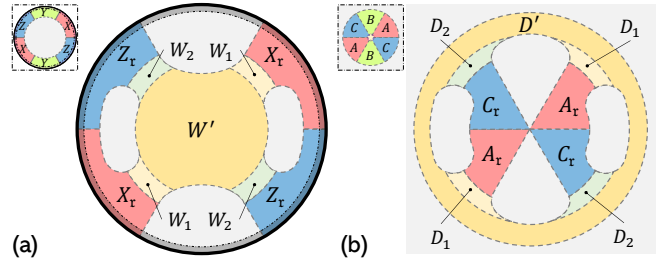


FIG. 15. Partitions of the residual term, $J(Z_\tau, W_\tau, X_\tau)$ and $J(C_\tau, D_\tau, A_\tau)$.

and, by plugging into $J(Z_\tau, W_\tau, X_\tau)$, we obtain

$$\begin{aligned} J(Z_\tau, W_\tau, X_\tau) &= i\langle [K_{(ZW)_\tau}, K_{(XW)_\tau}] \rangle \\ &= J(Z_\tau, W_2, W_\tau \setminus W_2) + J(W_\tau \setminus W_1, W_1, X_\tau) \\ &= 0. \end{aligned}$$

In the second and last line, we use the two properties of the modular commutator in Ref. [9]. In the second line, we use that if any of the subsets of the modular commutator is empty, the modular commutator vanishes:

$$J(\emptyset, B, C) = J(A, \emptyset, C) = J(A, B, \emptyset) = 0. \quad (\text{D4})$$

In the last line, we use that if the underlying state is a quantum Markov state, the modular commutator vanishes:

$$I(A : C|B) = 0 \implies J(A, B, C) = 0. \quad (\text{D5})$$

We can also prove the absence of the bulk residual term similarly. Consider the bulk residual term $J(C_\tau, D_\tau, A_\tau)$ in Fig. 15(b) and let $D_\tau = D_1 D_2 D'$. Then, we have

$$\begin{aligned} J(C_\tau, D_\tau, A_\tau) &= i\langle [K_{(CD)_\tau}, K_{(DA)_\tau}] \rangle \\ &= J(C_\tau, D_2, D_\tau \setminus D_2) + J(D_\tau \setminus D_1, D_1, A_\tau) \\ &= 0, \end{aligned}$$

where the properties of the modular commutator and the decomposition of the modular Hamiltonian are used:

$$\begin{aligned} K_{(CD)_\tau} &= K_{C_\tau D_2} + K_{D_\tau} - K_{D_2} \\ K_{(AD)_\tau} &= K_{A_\tau D_1} + K_{D_\tau} - K_{D_1}. \end{aligned}$$

We emphasize that this argument for the invertible bulk is applicable quite generally. Therefore, the additivity of the modular commutator manifests as long as the bulk is invertible and the subsystem is sufficiently larger than the bulk correlation length.

2. Discussion: non-invertible bulk

In a topologically ordered system, there is in fact a state for which the additivity of the modular commutator

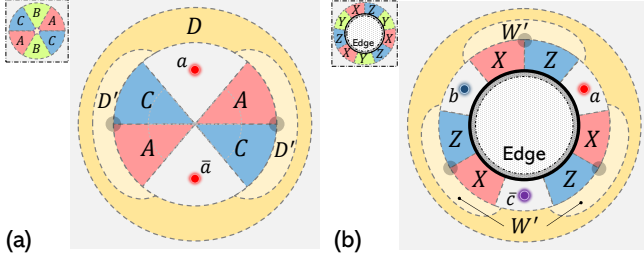


FIG. 16. The modular commutator of the pizza partitions in the non-invertible system. (a) An ensemble of the states containing anyons (a, \bar{a}) , where \bar{a} is anti-charge of topological charge a . Anyons are located in the subsystem B . (b) An maximum entropy ensemble of anyons (a, b, \bar{c}) that fuse into vacuum, where a and b fuse into c . The state $\tilde{\tau}$ satisfies $I(ZX : W \setminus W' | W')_{\tilde{\tau}} = 0$.

does hold. In the entanglement bootstrap program [28], certain *merged states* can be such states. A merged state is a maximum entropy state locally consistent with the ground state (or vacuum state, σ). In anyon theory, a merged state can be considered as a maximum entropy mixture containing anyons.

For example, consider a merged state on the bulk subsystem CDA as shown in Fig. 16(a). A merged state of our interest, say τ , is a maximum entropy state such that

$$I(CA : D \setminus D' | D')_{\tau} = 0. \quad (\text{D6})$$

In entanglement bootstrap, such a state can be generated by merging the states on disk and annulus, whose resulting subsystem is the two-hole disk [32]. In the context of anyon theory, an ensemble on CDA that has anyons (a, \bar{a}) in the holes (B) with probability $p_{a\bar{a}}^1 = d_a^2 / \mathcal{D}^2$ satisfies such conditional independence. Here, d_a is quantum dimension of anyon a and $\mathcal{D} = \sqrt{\sum_{a \in \mathcal{C}} d_a^2}$ is total quantum dimension over anyon superselection sector \mathcal{C} .

For this merged state (τ), the modular commutator

$J(C, D, A)_{\tau}$ is

$$\begin{aligned} J(C, D, A)_{\tau} &= J(C, D', A)_{\sigma} \\ &= 2 \times \frac{\pi}{3} c_- + J(C_{\tau}, D'_{\tau}, A_{\tau})_{\sigma}, \end{aligned} \quad (\text{D7})$$

where we use the conditional independence of the maximum entropy state, $I(C : D \setminus D' | D')_{\tau} = 0$ and $I(A : D \setminus D' | D')_{\tau} = 0$, in the first line and the additivity formula in the second line. The residual term vanishes $J(C_{\tau}, D'_{\tau}, A_{\tau})_{\sigma} = 0$ because the subsystems are disk-like region. Thus, we have $J(C, D, A)_{\tau} = 2 \times \frac{\pi}{3} c_-$.

Similarly, the additivity of the modular commutator manifests for a maximum entropy state, say $\tilde{\tau}$, on the edge pizza partition. For example, consider the subsystem ZWX on a disk as shown in Fig. 16(b). If the underlying state is a maximum entropy state such that $I(ZX : W \setminus W' | W')_{\tilde{\tau}} = 0$, we have

$$J(Z, W, X)_{\tilde{\tau}} = J(Z, W', X)_{\sigma} = -3 \times \frac{\pi}{3} c_-. \quad (\text{D8})$$

Note that the maximum entropy state $\tilde{\tau}$ can also be expressed as an ensemble containing anyons [Fig. 16(b)].

Therefore, if one proves that the modular commutator is invariant even in the presence of anyons, then the geometric additivity of the modular commutator is also proven

$$J(C, D, A)_{\tau} \stackrel{?}{=} J(C, D, A)_{\sigma} \quad (\text{D9a})$$

$$J(Z, W, X)_{\tilde{\tau}} \stackrel{?}{=} J(Z, W, X)_{\sigma} \quad (\text{D9b})$$

by using the identity, $J(C, D, A)_{\sigma} = J(A, B, C)_{\sigma}$ and $J(Z, W, X)_{\sigma} = J(X, Y, Z)_{\sigma}$. Thus, examining whether the modular commutator on the *pizza partition* remains invariant in the presence of anyons may be one of the strategies for proving the additivity of the modular commutator, even in non-invertible systems. We leave it as future work.